Title: The cellular and behavioral blueprints of chordate rheotaxis.

Authors: Oleg Tolstenkov[1*], Ayumi Ozawa[2*], Célestine Allombert-Blaise[1], Jørgen Høyer[1], Tetsuya Hiraiwa[3], Marios Chatzigeorgiou[1*]

Affiliations:

[1] Michael Sars Centre, Faculty of Science and Technology, University of Bergen, Norway

[2] Center for Mathematical Science and Advanced Technology, Japan Agency for Marine-Earth Science and Technology, Japan

[3]Institute of Physics, Academia Sinica, Taiwan

*Corresponding Authors Email: ozawaa@jamstec.go.jp, Oleg.Tolstenkov@uib.no, Marios.Chatzigeorgiou@uib.no

Abstract:
The oceans are filled with life-forms exhibiting complex adaptations to help navigate fluid environments and take advantage of fluid motion to locomote and disperse. However, the neuronal and behavioral underpinnings of navigating in fluid environments outside vertebrates are poorly understood.
We present behavioral and computational modelling-based evidence that the pre-vertebrate chordate *Ciona intestinalis* actively modulates its heading and angular velocities to counter oncoming flows and perform positive rheotaxis.
We demonstrate that a distributed network of ciliated peripheral sensory neurons is responsible for sensing hydrodynamic information such as flow velocity and direction. Pharmacological removal of sensory cilia impedes rheotactic behavior and reduces stimulus evoked neuronal activity.
Whole-brain calcium imaging experiments reveal that the central nervous system of *Ciona* can encode the onset and offset of flow, flow direction, and flow velocity, suggesting that miniature chordate brain is capable of surprisingly sophisticated computations.

Main Text:

The movement of organisms from one location to another has been a fundamental driving force of ecological and evolutionary processes since the beginning of life on Earth(*1-3*). A broad range of species, which include flying and swimming organisms are almost continuously subjected to stronger or weaker flows of the air or water currents respectively. Therefore, for animals that swim or fly, their movement is not only influenced by their locomotion but also by the motion of the fluid they are immersed in(*4-6*). Consequently, animals that are involved in goal-oriented swimming or flying are faced with the requirement to utilize sensory and behavioral mechanisms that enable them to detect directional flows and correct their locomotion to profit from favorably directed flows or counter opposing flows(*7*).

Paleontological records from the Ediacaran biota suggest that in aquatic environments, rheotaxis may have been one of the earliest mechanisms that evolved to exploit or counter turbulent flows(*3, 8-10*).

Rheotaxis is a form of oriented movement exhibited by an organism in response to a current of fluid(*11-20*). Rheotactic behavior has been observed in organisms of very different dimensions, from millimeter long fish larvae(*16, 18*) all the way to meters long sharks(*12*) including the enormous filter-feeding whale sharks (*Rhincodon typus*)(*21*). The sensory basis of rheotaxis has been explored in fish using models like goldfish (*Carassius auratus)* and zebrafish (*Danio rerio*). Vision was regarded a key sense to detect whole-field motion relative to their frame of reference(*11, 22-25*) even though the idea of visual dominance has been challenged(*26*). Indeed, aquatic organisms can perform rheotaxis in the absence of visual cues by leveraging mechanosensory information detected by the lateral line(*13, 16, 18, 27-30*). More recently, the idea of multisensory control of rheotaxis has been put forward(*17, 31*). Investigations of the circuitry architecture underlying flow sensing in fish have shown that lateral line ganglia respond to the direction of flow, while different brain regions encode flow onset, speed and accumulated displacement of flow(*27, 32*). Outside aquatic vertebrates rheotaxis remains a understudied behavior (*33-38*), while the evolution of the behavior and the underlying molecular and neuronal mechanisms remain to date unmapped.

To address these gaps in our knowledge we must turn our attention to marine invertebrate chordates that almost 500 million years ago, started to colonize the oceans, using their dispersing larvae which swam in the water column to reach new habitats. The ability to navigate in the water column and the capacity to hitchhike favorably directed flows or to counter opposing flows will likely have been critical to their ability to spread in the oceanic environment. Evidence of motility and associated behavior of extant invertebrate chordates are generally rare in the fossil record. Therefore, we must study extant invertebrate chordates like tunicates whose distribution in natural marine habitats has been attributed to water flow(*39-41*).

However, the question of whether invertebrate chordates like the tunicates are capable of rheotaxis remains to date unanswered. More generally the behavioral algorithms that zooplanktonic organisms employ to perform rheotaxis and the underlying neuronal mechanisms are largely unknown. Importantly it is unclear how zooplanktonic larvae encode sensory cues (e.g. hydromechanical cues) in their brains to reach the adaptive decision to swim with or against the direction of the water flow.

Here, we leverage the zooplanktonic swimming larva of the tunicate *Ciona intestinalis*, with an extremely streamlined nervous system composed of only 231 cells (*42*), to investigate the behavioral and neuronal bases of rheotaxis.

Using quantitative behavior analysis and mathematical modeling we find that *Ciona* larvae exhibit active rheotaxis, using a novel behavioral algorithm, based on modulating their heading and angular velocities. Using Ca^{2+} imaging coupled to directional flow stimulation we

demonstrate that polymodal sensory neurons which are distributed across the surface of the larval trunk show directional selectivity to oncoming current. By combining whole-brain Ca^{2+} imaging and microfluidics we determine that the larval midbrain is encoding flow onset and offset, while the hindbrain which is processing flow velocity information. By investigating both behavioral and neuronal responses, we provide new insights into the mechanisms underlying flow sensing in marine invertebrates.

***Ciona* larvae exhibit positive rheotaxis by modulating heading and angular velocities.**
To investigate the ability of *Ciona intestinalis* larvae to perform rheotaxis we designed a rheotaxis setup capable of exposing multiple *Ciona* larvae to flowing streams whose velocity could be adjusted (Fig. 1A-C). The larvae were imaged under near-infrared light to avoid visible light interference(*43-46*). Using both trajectory density analysis and 2D markerless pose estimation (*47*) (Fig. 1D and E), we were able to track and quantify the larvae's motion. When exposed to a range of flow stimulus strengths (1-3mm/s), we observed that *Ciona* larvae were either swept from the flow or they exhibited positive rheotaxis (Fig. 1F and 1G; fig. S1E). Quantification of larval swimming revealed that the mean rheotaxis probability (probability of upstream orientation) was significantly higher when animals were challenged with a 2mm/s (two body lengths/s) flow stream compared to static (0 mm/s) water (Fig. 1H; fig. S1A, S1C, and S1G; S1F, and S1I for other flow strengths). This positive rheotaxis response was characterized by a significant increase in average heading velocity (fig. S1B, S1D, S1L, S1N, and S1J; fig. S2A), while angular velocity, a metric of rotational velocity about the center of mass of the larva was reduced when swimming longer distances suggesting more direct swimming (fig. S1M and fig. S2A), while the averaged mean angular velocity did not change (fig. S1K, S1O), indicating the larvae's ability to effectively compensate for displacements induced by the flow of the water. To further characterize the phenotype, we quantified the density of actively swimming *Ciona* larvae body vectors orientation. Under no flow conditions we observed a uniform density across all orientations (Fig. 1I, blue density). When we introduced a flow stimulus, we saw a prominent peak at 90° (upstream) and a smaller peak at 270° (downstream) suggesting that the larvae aligned primarily against and secondarily with the direction of flow (Fig. 1I, red density). Close inspection of swimming trajectories suggested that larvae in static sea water performed mostly localized circular swimming akin to what has been shown previously for spontaneously swimming larvae(*48*), in contrast to larvae exposed to a 2mm/s flow which moved upstream following a helical swimming pattern (Fig. 1J).

To quantitatively investigate how a *Ciona* larva can achieve rheotaxis while executing a helical trajectory, we constructed a computational framework to simulate the dynamics of swimming *Cionas*. Here, we simply assume that, at the time t, a *Ciona* is located at the position $\big(x(t), y(t)\big)$ with body vector orientation $\theta(t)$, and the equation of motion is given by

$$\frac{d}{dt}\begin{bmatrix} x(t) \\ y(t) \end{bmatrix} = v\big(\theta(t); f(t)\big)\begin{bmatrix} \cos\theta(t) \\ \sin\theta\,(t) \end{bmatrix} + \begin{bmatrix} \xi^x(t) \\ \xi^y(t) \end{bmatrix}, \tag{1a}$$

$$\frac{d\theta(t)}{dt} = \omega\big(\theta(t); f(t)\big) + \xi^\theta(t), \tag{1b}$$

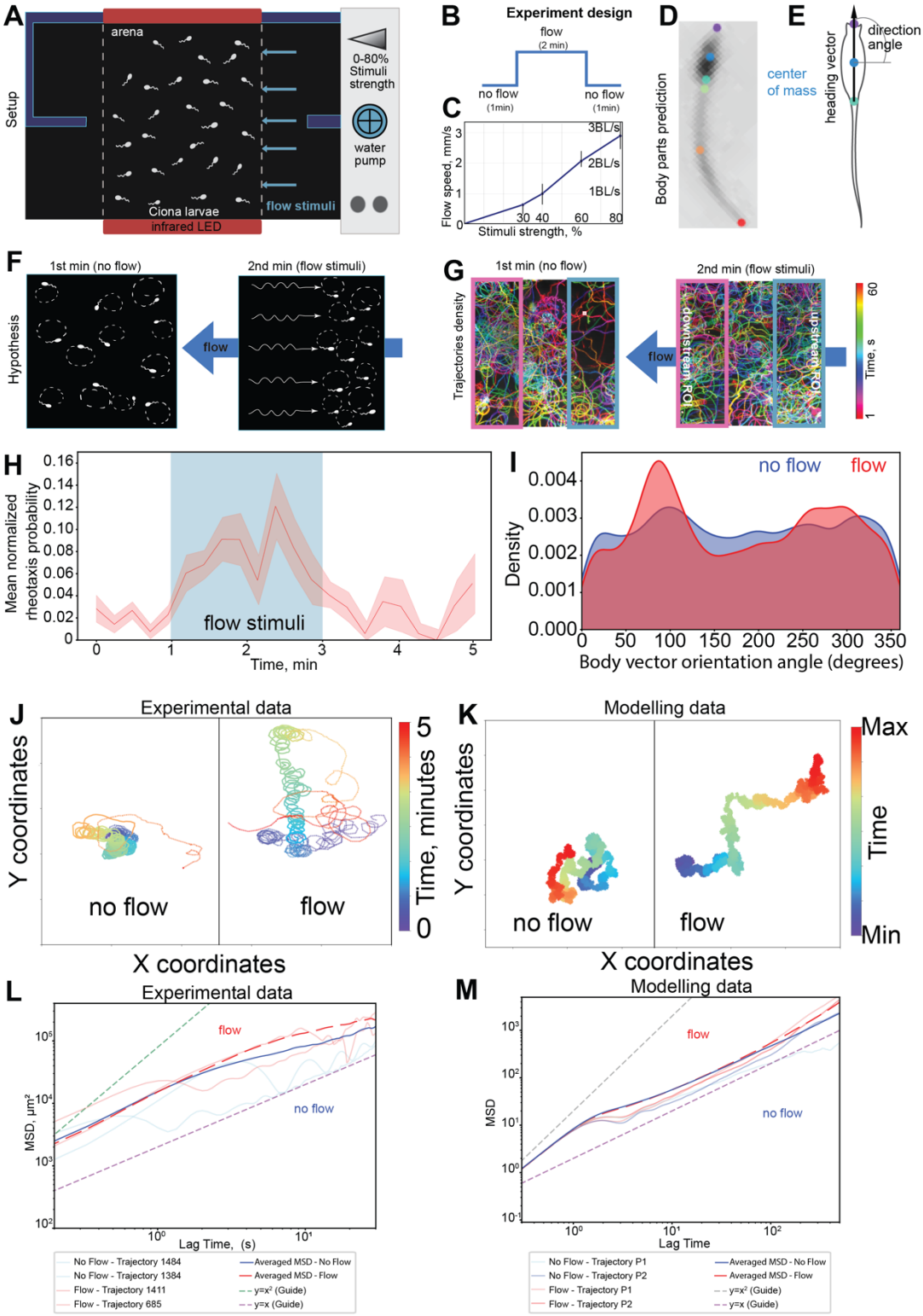
A
Setup
arena
0-80% Stimuli strength
water pump
Ciona larvae
infrared LED
flow stimuli
B
Experiment design
flow
(2 min)
no flow
(1min)
no flow
(1min)
C
Flow speed, mm/s
3BL/s
2BL/s
1BL/s
Stimuli strength, %
D
Body parts prediction
center of mass
E
heading vector
direction angle
F
Hypothesis
1st min (no flow)
2nd min (flow stimuli)
flow
G
Trajectories density
1st min (no flow)
2nd min (flow stimuli)
downstream ROI
upstream ROI
Time, s
H
Mean normalized rheotaxis probability
flow stimuli
Time, min
I
no flow
flow
Density
Body vector orientation angle (degrees)
J
Experimental data
Y coordinates
X coordinates
no flow
flow
Time, minutes
K
Modelling data
Y coordinates
X coordinates
no flow
flow
Max
Time
Min
L
Experimental data
MSD, μm²
Lag Time, (s)
flow
no flow
No Flow - Trajectory 1484
No Flow - Trajectory 1384
Flow - Trajectory 1411
Flow - Trajectory 685
Averaged MSD - No Flow
Averaged MSD - Flow
y=x² (Guide)
y=x (Guide)
M
Modelling data
MSD
Lag Time
flow
no flow
No Flow - Trajectory P1
No Flow - Trajectory P2
Flow - Trajectory P1
Flow - Trajectory P2
Averaged MSD - No Flow
Averaged MSD - Flow
y=x² (Guide)
y=x (Guide)

Fig. 1 *Ciona* larvae exhibit positive rheotaxis by modulating heading and angular velocities.
(**A**) Schematic of the rheotaxis setup. (**B**) Experimental protocol timeline: 1 min. of static water, followed by 2 min. of exposure to flow, followed by 2 min. of static flow. **(C)** A calibration plot showing the flow stimulus strength (% of maximum flow strength) as a function of water flow velocity in mm/s and *Ciona* body lengths (BL) per second. **(D)** A deep neural network (DNN) trained in DeepLabCut(*47*) was used to extract the locations of *Ciona* body parts from videos. The image shows the most likely locations for 6 labeled body parts of a *Ciona* larva. **(E)** Schematic of the labelled body parts used for establishing the larva's heading (body) vector and direction (orientation) angle between the heading vector and fixed coordinates of arena **(F)** Schematic illustrating the hypothesis of positive rheotaxis in swimming *Ciona* larvae. **(G)** The trajectory density of a representative experiment, alongside a schematic illustrating the measurement and comparison of mean grey values of animal trajectories in the upstream and downstream regions of interest (ROIs) under control (no flow) and flow stimulus conditions with 1 min duration for each condition. Trajectories are color-coded to represent different time points. **(H)** Mean rheotaxis probability under no flow conditions and 60% strength, i.e. 2mm/s. Solid line shows the mean probability value, shade indicates SEM. Blue vertical bar defines the flow stimulus presentation for the flow experiments. **(I)** Body vector orientation distributions under no flow (blue) and 60% flow (red) conditions for wild-type larvae. Animal trajectories for H and I were filtered based on speed (>1.2 mm/s) to exclude inactive larvae (Supplementary Fig. S1N). **(J)** Representative trajectories of swimming larvae exposed to no flow (static water) or flow at 2mm/s recorded in the rheotaxis setups (experimental data). **(K)** Representative trajectories which are the output of the mathematical model. For trajectories in J and K color-coding corresponds to temporal progression (blue to red). **(L and M)** Mean square displacement (MSD) based on experimental data (L) and computational simulation data (M) under no flow (solid blue curve) or flow stimulus (dotted red curve) conditions showing a shift (transition) of the movement pattern from a more diffusive regime (purple guideline) characterized by frequent reorientations to a more ballistic regime (green guideline) with more directed trajectories in the flow condition.

where $v(\theta; f)$ and $\omega(\theta; f)$ represent the heading speed and angular velocity, which in general can depend on the body vector orientation θ and the flow condition f, the parameter indicating whether the flow stimulation is on or off; $f = 1$ ($f = 0$) in the presence (absence) of the flow. These functions can reflect the experimental observations. Note that, nicely, the mathematical analysis showed that $\omega(\theta)$ should be proportional to $1/h(\theta)$ (Supplementary Materials), which help us to set $\omega(\theta)$ from the data. We assume that the system is exposed to noises, which are represented as $\xi^x(t)$, $\xi^y(t)$, and $\xi^\theta(t)$ (see Supplementary Materials for more details).
Experimental results show that $v(\theta; f)$ and $\omega(\theta; f)$ vary depending on the surrounding flow and the body vector orientation (fig. S4H). Specifically, the two peaks at approximately $90°$ and $270°$ in the body vector orientation distribution $h(\theta)$ under flow condition (Fig. 1I) indicate that the larvae tend to change their orientation slowly when they direct these angles (fig. S2B). Furthermore, in the presence of flow stimulation, the heading speed of actively swimming larvae tends to be smaller when the body vector orientation θ is close to $90°$ and $270°$. We incorporate in our model these responses to the flow by setting the functions $v(\theta; f)$ and $\omega(\theta; f)$ to match to the experimental data (fig. S2B and S4H).
We confirmed that the result of the computer simulations based on this model indeed yielded trajectories that resembled the experimental animal center of mass trajectories (Fig. 1J and K,

fig. S2C). Additionally, use of the mean square displacement (MSD) metric (*49*) suggested that experimental (Fig. 1L) and model-derived data (Fig. 1M) exhibit comparable movement dynamics in the following sense: (1) on a sufficiently short time scale, the slope of the MSD plotted on a log-log scale is approximately 1, indicating that the dynamics is diffusive, (2) on a larger timescale, the slope of the MSD under the flow condition is larger than 1. Thus, the MSD analysis supports the rheotaxis hypothesis, showing the increased displacement and more directed, ballistic movement under flow conditions compared to more random, diffusive behavior in no-flow conditions (Fig. 1L and 1M; fig. S1P).

These results indicate that the realization of the rheotaxis while drawing a helical trajectory can be explained by the modulation of heading speed and angular velocity depending on the relative angle of the body orientation to the flow direction and support the validity of our mathematical framework. To further resolve the contributions of the heading speed and angular velocity in achieving rheotaxis, we use the model simulated here as a control for further investigation under "one-sided" conditions. Namely, we compared the control with the following two cases: (1) the angular-velocity-only condition, where $\omega(\theta; f)$ is the same as the control while $v(\theta; f) = v_0$, and (2) the heading-speed-only condition, where $v(\theta; f)$ is the same as the control while $\omega(\theta; f) = \omega_0$. The resultant MSD behaves similarly to the control when only the $\omega(\theta; f)$ follows the case with flow, whereas it does not when only the heading speed follows the case with flow (Supplemental Material; fig. S2D-S2F). We thus conclude that, while both heading speed and angular velocity are modulated by flow, *Ciona* rheotaxis is caused specifically by the modulation of the angular velocity.

While the principal mechanism of the rheotaxis is the modulation of the angular velocity, further numerical investigation by partly modifying $v(\theta; f)$ indicated that the modulation of the heading speed around $\theta = 270°$ enhances the rheotaxis. See Supplemental Materials for more details.

A distributed network of polymodal sensory neurons detects changes in water flow.

Despite the prevalence of rheotactic behavior in nature, little is known about the underlying neural mechanism outside a handful of model organisms(*16, 27, 32*). We hypothesized that *Ciona* employs its miniaturized nervous system to perceive and encode changes in flow which result in rheotactic behavior. *Ciona* is equipped with 54 peripheral sensory neurons(*50*), distributed across the trunk and tail of the larvae. These neurons are equipped with cilia or ciliary neurites that protrude into the tunic(*51, 52*). They function either as primary mechanosensory neurons(*53*) or as polymodal sensory neurons capable of responding to mechanical and chemical cues important for larval settlement and metamorphosis(*54-57*).

To test the ability of the sensory cells to detect water flow, we conducted experiments using a perfusion pencil-based flow system (Fig. 2A) combined with calcium imaging in larvae expressing the calcium indicator GCaMP6s(*58*) using the *Cii.pc2* promoter which labels robustly peptidergic neurons, which includes the majority of the peripheral nervous system and a subset of CNS neurons(*54, 59*) (Fig. 2B and C and fig. S2).

Among the various types of sensory cells, the papillae sensory neurons (PSNs), the rostral trunk epidermal neurons (RTENs) and apical trunk epidermal neurons (ATENs) responded to flow (Fig. 2D-I and fig. S3A to C). An unexpected feature of these Ca^{2+} responses is that their strength, as quantified by the area under the curve, showed a directional dependency on the flow direction (Fig. 2D-I), suggesting that *Ciona* epidermal sensory neurons can encode the directionality of flow stimuli.

To investigate the downstream processing of flow stimuli, we performed whole-brain imaging of *Ciona* larvae using a microfluidics device (Fig. 2J), with a nuclear localized GCaMP6s expressed pan-neuronally(*54*) (Fig. 2K). Interestingly, exposing larvae to a two-flow stimuli

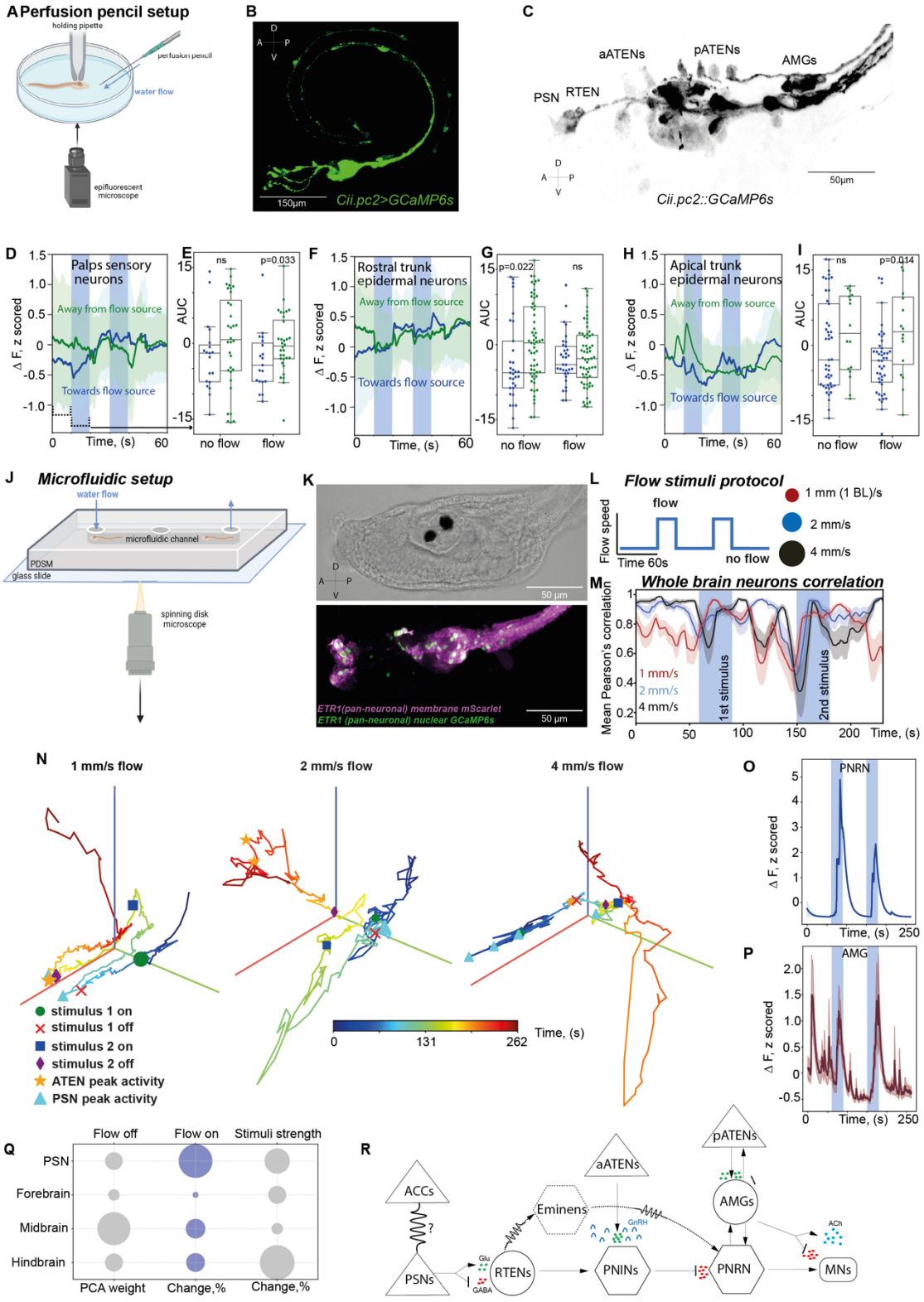
A Perfusion pencil setup
holding pipette
perfusion pencil
water flow
epifluorescent microscope
B
150µm
Cii.pc2>GCaMP6s
C
aATENs
pATENs
AMGs
PSN
RTEN
50µm
Cii.pc2::GCaMP6s
D
Palps sensory neurons
Away from flow source
Towards flow source
Δ F, z scored
Time, (s)
E
ns
p=0.033
AUC
no flow
flow
F
Rostral trunk epidermal neurons
G
p=0.022
ns
H
Apical trunk epidermal neurons
I
p=0.014
J Microfluidic setup
water flow
microfluidic channel
PDSM
glass slide
spinning disk microscope
K
50 µm
ETR1(pan-neuronal) membrane mScarlet
ETR1 (pan-neuronal) nuclear GCaMP6s
L Flow stimuli protocol
flow
Flow speed
Time 60s
no flow
1 mm (1 BL)/s
2 mm/s
4 mm/s
M Whole brain neurons correlation
Mean Pearson's correlation
1 mm/s
2 mm/s
4 mm/s
1st stimulus
2nd stimulus
N
1 mm/s flow
2 mm/s flow
4 mm/s flow
stimulus 1 on
stimulus 1 off
stimulus 2 on
stimulus 2 off
ATEN peak activity
PSN peak activity
Time, (s)
O
PNRN
P
AMG
Q
Flow off
Flow on
Stimuli strength
PSN
Forebrain
Midbrain
Hindbrain
PCA weight
Change,%
R
ACCs
PSNs
RTENs
Eminens
aATENs
PNINs
pATENs
AMGs
PNRN
MNs
Glu
GABA
GnRH
ACh

Fig. 2 A distributed network of polymodal sensory neurons detects changes in water flow and engages midbrain and hindbrain neurons to compute flow features.

(**A**) Schematic of the perfusion pencil setup used to deliver flow stimuli while performing Ca^{2+} imaging. (**B**) Representative maximal projection of a *Ciona* larva expressing *Cii.pc2::GCaMP6s* in peptidergic neurons of the CNS and Peripheral Nervous System (PNS) **(C)** Max projection of trunk neurons labelled by *Cii.pc2::GCaMP6s* in *Ciona* larvae, the polymodal papillae sensory neurons (PSNs), the rostral trunk epidermal neurons (RTENs), the anterior/ posterior apical trunk epidermal neurons (aATENs & pATENs) and the ascending motor ganglion interneurons (AMGs). **(D-I)** Mean Ca^{2+} responses and quantification of area under the curve (AUC) to directional flow stimuli, showing directionally selective activation patterns of selected sensory cell types when they are positioned towards or away from the flow source. The solid line indicates mean response; shaded areas show standart deviation SEM. Blue intervals indicate flow stimulation. Data points in (E,G,I) represent individual neurons. Dotted lines in D show the time intervals for mean quantative comparison. Statistical analysis in (E, G and I) was performed using the Mann-Whitney U test. **(J)** Schematic of the microfluidic setup used for whole-brain Ca^{2+} imaging. **(K)** Brightfield and maximal confocal projection of the trunk region of a representative transgenic *Ciona* larva which was used for whole-brain imaging expressing *Cii.Etr-1>nls::GCaMP6s::nls* (green) and *Cii.Etr-1>Lck-mScarlet* (magenda). **(L)** Flow stimuli protocol that was applied to *Ciona* larvae in the microfluidic chip. Two flow stimuli were delivered per animal. **(M)** Mean Pearson's correlation of whole-brain activity calculated for medians of all cells with the 30 frames rolling window showing that repeated stimulus presentation enhances brain synchronization, shaded areas show 95% confidence interval. **(N),** Temporal progression of whole-brain Ca^{2+} activity trajectories at different flow speeds (1, 2, 4 mm/s). **(O),** Average trace of multiple Ca^{2+} responses from a class of premotor interneuron called peripheral relay neuron (PNRN). (blue bars indicate stimulus delivery interval). **(P)** Average Ca^{2+} responses from a class of peripheral motor neurons (AMGs). **(Q)** Quantitative summary of the impact of different brain regions impact on the processing of different parameters of flow stimuli. Ciona neurons were classified into brain regions as follows: PNS (PSNs, RTENs, ATENs, and DCENs), forebrain (PRs and coronet cells), midbrain (PNSRN, PRRN, ANTRN, and ANT), and hindbrain (AMG, PMG, and MN). PCA absolute loading weights were summed for each neuron type and then aggregated at the brain region level and time period. Changes in PCA weights from the no flow to flow condition and across different flow speeds are represented in the bubble plot. **(R)** Putative neural circuitry transmitting flow cues from the periphery to the central nervous system and motor neurons, integrating sensory cell inputs and whole-brain imaging results. The signal propagates through the nervous system in accordance with predictions of the connectome. Glutamatergic/Gabaergic sensory cells (triangular cells) excite midbrain and hindbrain interneurons and relay neurons (polygons: Eminens, PNINs, PNRNs, circle: AMGs), which in turn balance excitatory and inhibitory signaling via acetylcholine (ACh) and GABA release to regulate the motorneurons (MNs, rectangle shape) of *Ciona*. Neurotransmitters and neuromodulators are assigned based on previous studies(*74-80*).

protocol (Fig. 2L) we found that repeated presentation of the flow stimulus resulted in higher level of synchronization of brain-wide neuronal activity (Fig. 2M). The speed of the flow cue with which the larvae were stimulated (we tested 1mm/s, 2mm/s and 4mm/s), was also encoded at a brain-wide level as it can be inferred by the qualitatively distinct brain activity trajectories elicited by the different flow speeds (Fig. 2N). Downstream integrating premotor interneurons located in the midbrain (PNRN) and hindbrain (AMGs), played a major role in this processing (Fig. 2O, 2P and fig. S3D). These neurons are highly relevant for integrating rheotactic stimuli information since the PNRN receives indirect inhibitory input from the RTENs and the AMGs receive direct input from the pATENs(*42, 50, 60*).

To estimate the contribution of *Ciona*'s different brain regions in the stimuli information processing we quantified and grouped absolute PCA loading for all individual cells according to the anatomical region they were in (Fig. 2Q). We determined that the midbrain was encoding flow onset and offset, while the hindbrain was processing flow speed information transmitted by sensory neurons to the CNS (Fig. 2Q and R). Taken together our data suggest that *Ciona* senses flow using a distributed network of sensory neurons on the larval trunk and uses its midbrain and hindbrain circuitry to compute flow features like stimulus onset/offset and strength.

Ciliated sensory neurons in the trunk and tail of the larvae are required for rheotaxis

In zebrafish, ablation of cilia on superficial neurons in the neuromast ridges significantly reduces rheotaxis ability (*16*). To test the role of ciliated sensory neurons in *Ciona* larvae, we chemically ablated the cilia using chloral hydrate (*61*) (Fig. 3A-C). Loss of sensory cilia which protrude into the tunic resulted in a strong rheotaxis defect (Fig. 3D) including the reverse effect of the flow on heading and angular velocity compare to the wildtype (fig S4 A, B and D, E) and on the motion (fig S4 C). Upon the introduction of a flow stimulus control larvae performed a significantly higher number of upstream swims compared to downstream swims, thus exhibiting positive rheotaxis (Fig. 3E and F). In contrast chloral hydrate treated animals did not significantly switch from downstream to upstream swimming upon flow introduction (Fig. 3E and F). In addition, we quantified the density of *Ciona* larvae body vectors in chloral hydrate treated animals (Fig. 3G). Chloral hydrate treated animals similarly to controls showed a uniform distribution of body vectors in static water (no flow) (Fig. 1I; Fig. 3G). However, in contrast to controls in the presence of flow we observed only the 270° peak suggesting that the larvae were unable to orient themselves against the flow (Fig. 1I; Fig. 3G and fig S1H, I, J, K). Finally, we observed a decrease in the probability to swim upstream upon introduction of flow (Fig. 3H). We then decided to monitor Ca^{2+} responses to flow in the ciliated ATENs (located in the trunk of the animals) and the ciliated DCENs and VCENs located in tail. We found that chloride hydrate treatment eliminated flow induced Ca^{2+} responses in the ATENs but did not affect DCENs or VCENs responses (Fig. 3I, 3J and fig. S4F and G). Taken together our results suggest that ciliated sensory neurons in the trunk of the animals are required for positive rheotaxis.

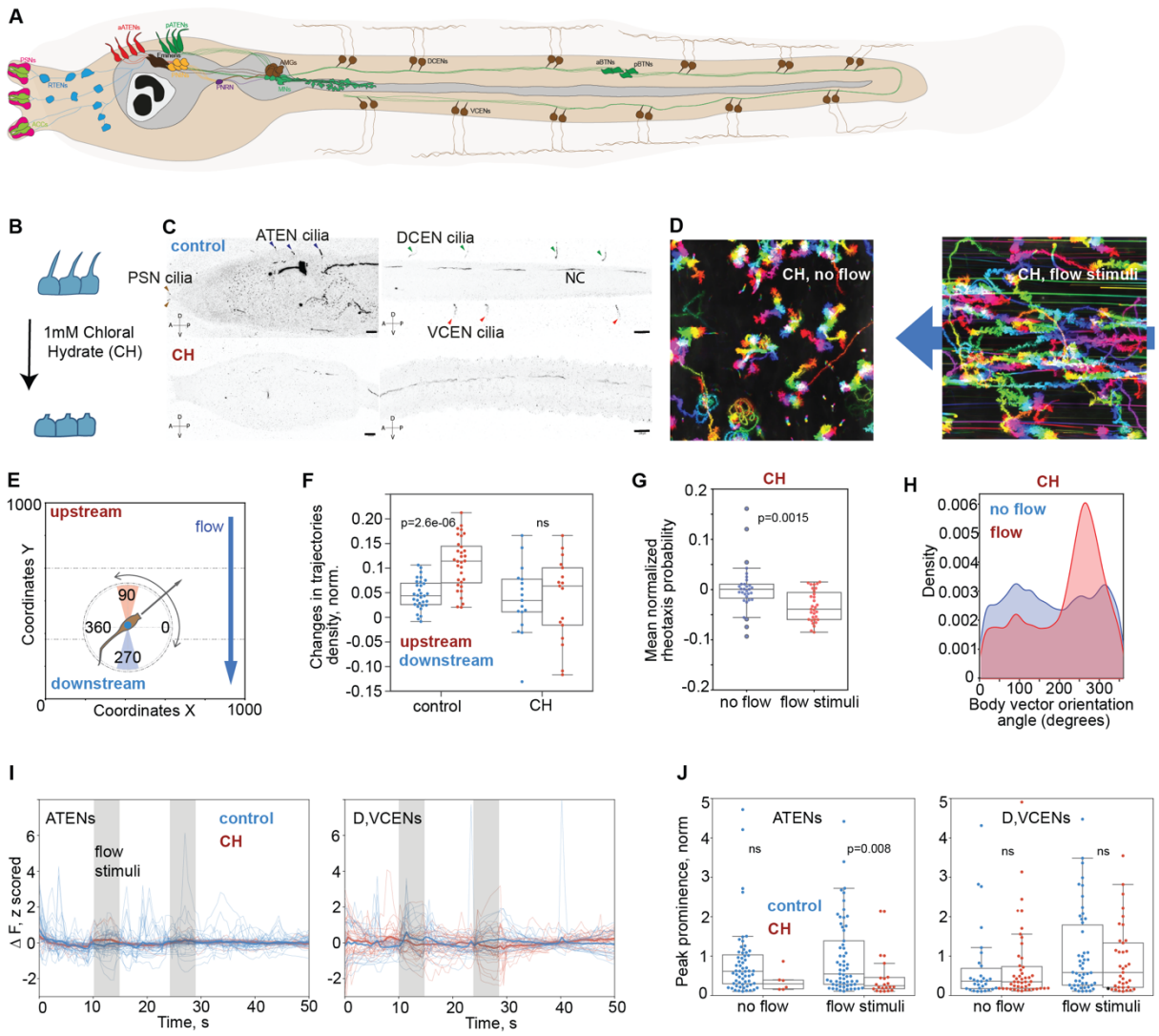

Fig.3 Trunk ciliated sensory neurons are required for positive rheotaxis.
(**A**) Schematic of a Ciona larva showing key ciliated neurons of the PNS and some important CNS neurons. (**B**) Schematic of the chloral hydrate (CH) treatment used to ablate sensory cilia. **(C)** Maximal projections of control and chloral hydrate treated larvae where trunk and tail sensory neuron cilia, as well as ependymal cell cilia in the nerve cord are stained with anti-tubulin antibody. **(D)** Trajectories of chloral hydrate treated larvae under no flow and flow conditions for 1 min (color-code indicates temporal progression). **(E)** Schematic illustrating the range of angles considered as upstream swimming (red shade) and downstream swimming (blue shade). **(F)** Quantification of change in upstream and downstream trajectories density in wildtype and Chloral hydrate treated groups. Data points in F and H are representing the means of individual experiments. **(G)** Body vector orientation distributions under no flow (blue) and flow (red) conditions for chloral hydrate treated larvae showing the loss of the upstream angles peak in the treated animals. **(H)** Quantification of the probability to perform positive rheotaxis under no flow and flow conditions for chloral hydrate treated larvae. **(I)** Ca^{2+} traces showing reduced response in response to flow stimuli, in apical trunk epidermal neurons (ATENs) following cilia ablation relative to negative controls, while tail sensory neurons (DCENs, VCENs) remained unaffected. **(J)** Quantification of normalized peak prominence of Ca^{2+} transients elicited by flow stimuli in ATENs and DCENs/VCENs of control and chloral hydrate treated larvae. Data points in J are representing the individual neurons. For panels F, G, J we used a Mann-Whitney U test for statistical analysis.

Discussion

This study provides a systems level understanding of a miniature nervous system in a zooplanktonic invertebrate chordate larva and how it operates in marine habitats with dynamic fluid flows.

We establish that *Ciona* larvae can perform positive rheotaxis using helical swimming. Our experiments showed that a relatively complex behavior can be executed by a larva with such a small nervous system by using a surprisingly simple behavioral algorithm. Zebrafish use a different but equally simple behavioral algorithm to perform rheotaxis using flow velocity gradients(*18*). The rheotactic behavioral regime of *Ciona* differs also from that of other zooplanktonic organisms such as calanoid copepods (*Eurytenora affinis*), which use a mix of frequent jumps and turbulent transport(*38*). The ability to detect and respond to different flow strengths may confer to *Ciona* the ability to detect and perform fast maneuvers to escape from predators as is the case for planktonic copepods(*62*). Notably, even if most of the hatched larvae are swept from the water flow, the ability of a significant fraction to perform active rheotaxis may carry a strong fitness benefit for *Ciona* because it would enable these small zooplanktonic organisms to retain the advantages of self-locomotion under varying strength and direction flow conditions. In doing so it would give *Ciona* the capacity to move to a suitable habitat for settlement or to control their distribution despite strong hydrodynamics, while maintaining the diffusive properties of their motion. The result would be an ability to regulate the dispersal of the population akin to what has been documented for calanoid copepods(*38*). This behavioral trait would provide a selective advantage even when the difference in diffusivity is small(*63*).

This study has elucidated the sensory mechanisms and downstream processing circuit underlying flow sensation. We found that *Ciona* leverages a network of ciliated trunk epidermal sensory neurons which are distributed along the rostral/caudal and mediolateral axes to sense flow. We establish that these superficial sensory neurons detect flow over the surface of trunk and have a suitable spatial distribution to signal the direction and strength of flow, thus contributing to the detection of local differences in flow across different parts of the trunk. Epidermal neurons form a unique outer body dendritic network in the ascidian larval tunic (*52*). Interestingly they express differentiation gene batteries that are conserved with those of lateral line hair cells (*64*). In addition, an ancestral relationship to the chordate PNS has been postulated on the grounds that these cells deliver overlapping input to the CNS and that they are distributed in an antero-posterior direction(*65*). We and others have recently shown that these epidermal sensory neurons detect both mechanical and chemical cues (*54, 55*). While lateral line hair cells in vertebrates were thought to be exclusively mechanosensory, a recent study raises the possibility that they are polymodal, since they are also capable of sensing chemical cues(*66*). Taken together, our findings suggest that the sensory cells employed by vertebrates to sense flow may have evolved earlier in the chordate lineage.

Through whole brain-calcium imaging we have identified at least two sensorimotor integration sites in the CNS, namely the PNRN neuron located in the midbrain and the AMGs located on the dorsal side of the hindbrain. Interestingly, the zebrafish hindbrain has been identified as the brain location where water-flow direction selective cell clusters are located(*27, 32*). In goldfish, midbrain and hindbrain clusters responded to various hydrodynamic stimuli(*67, 68*). We find that the peripheral nervous system and the hindbrain are two primary sites where flow strength is encoded and decoded in the *Ciona* larval nervous system. Early studies based on anatomical features, suggested that the peripheral DCENs and VCENs are initiating swimming or acting as proprioceptors during swimming(*69*). While the DCENs may not contribute to sensing flow stimuli per se, they may provide tail postural information to their postsynaptic targets the AMG neurons, suggesting that the AMGs are key integrators of rheotactic information and self-movement.

Typically, animal brains including that of *Ciona* larvae transition between dynamic internal states in response to tasks such as foraging or chemosensation(*54, 70-73*). We show that *Ciona* has two distinct phases when engaging and disengaging in flow sensing, suggesting that state-encoding neural populations may be responsible for the initiation and termination of the rheotactic behavior. The emerging picture is that invertebrate chordates and teleost fish employ evolutionary conserved brain regions and neural mechanisms for sensorimotor transformation during rheotaxis.

Acknowledgments
We would like to thank Shobhan Dev Mandal for discussions on the computational modeling aspects of this manuscript. We would also thank members of the Chatzigeorgiou lab for feedback on the manuscript.

Funding
Research Council of Norway: 339399 (M.C.) and 234817 to the Michael Sars Centre. JAMESTEC Young Research Fellow Research Grant (A.O.)

Author contributions
Conceptualization: O.T., M.C.; Methodology: O.T., M.C., A.O., T.H.; Data curation: O.T., A.O., C.A.B., J.H.; Investigation: O.T., A.O., C.A.B., J.H.; Visualization: O.T., A.O., M.C., C.A.B., J.H.; Resources: O.T., M.C.; Funding acquisition: M.C., A.O., T.H.; Project administration: M.C., T.H.; Supervision: M.C.; Writing – original draft: O.T., M.C.; Writing – review and editing: O.T., A.O., M.C., C.A.B., J.H., T.H.

Declaration of interests
The authors declare no competing interests.

REFERENCES

1. T. Alerstam, A. Hedenström, S. Åkesson, Long-distance migration: evolution and determinants. *Oikos* **103**, 247-260 (2003).
2. H. Dingle, V. A. Drake, What is migration? *Bioscience* **57**, 113-121 (2007).
3. B. M. Gibson *et al.*, Ancient life and moving fluids. *Biol Rev Camb Philos Soc* **96**, 129-152 (2021).
4. M. Gazzola, M. Argentina, L. Mahadevan, Scaling macroscopic aquatic locomotion. *Nature Physics* **10**, 758-761 (2014).
5. R. Dudley, *The Biomechanics of Insect Flight*
Form, Function, Evolution. (Princeton University Press, 2000).
6. S. D. Stupski, F. van Breugel, Wind gates olfaction-driven search states in free flight. *Curr Biol*, (2024).
7. J. W. Chapman *et al.*, Animal orientation strategies for movement in flows. *Curr Biol* **21**, R861-870 (2011).

8. J. R. Paterson, J. G. Gehling, M. L. Droser, R. D. Bicknell, Rheotaxis in the Ediacaran epibenthic organism Parvancorina from South Australia. *Sci Rep* **7**, 45539 (2017).
9. S. A. F. Darroch, I. A. Rahman, B. Gibson, R. A. Racicot, M. Laflamme, Inference of facultative mobility in the enigmatic Ediacaran organism Parvancorina. *Biol Lett* **13**, (2017).
10. F. J. Coutts, C. J. A. Bradshaw, D. C. García-Bellido, J. G. Gehling, Evidence of sensory-driven behavior in the Ediacaran organism Parvancorina: Implications and autecological interpretations. *Gondwana Research* **55**, 21-29 (2018).
11. E. P. Lyon, ON RHEOTROPISM. I. — RHEOTROPISM IN FISHES. *American Journal of Physiology-Legacy Content* **12**, 149-161 (1904).
12. R. F. Mathewson, E. S. Hodgson, Klinotaxis and rheotaxis in orientation of sharks toward chemical stimuli. *Comparative Biochemistry and Physiology Part A: Physiology* **42**, 79-84 (1972).
13. J. C. Montgomery, C. F. Baker, A. G. Carton, The lateral line can mediate rheotaxis in fish. *Nature* **389**, 960-963 (1997).
14. C. F. Baker, J. C. Montgomery, The sensory basis of rheotaxis in the blind Mexican cave fish, Astyanax fasciatus. *Journal of Comparative Physiology A* **184**, 519-527 (1999).
15. J. M. Gardiner, J. Atema, Sharks need the lateral line to locate odor sources: rheotaxis and eddy chemotaxis. *Journal of Experimental Biology* **210**, 1925-1934 (2007).
16. A. Suli, G. M. Watson, E. W. Rubel, D. W. Raible, Rheotaxis in larval zebrafish is mediated by lateral line mechanosensory hair cells. *PLoS One* **7**, e29727 (2012).
17. R. Olive *et al.*, Rheotaxis of Larval Zebrafish: Behavioral Study of a Multi-Sensory Process. *Front Syst Neurosci* **10**, 14 (2016).
18. P. Oteiza, I. Odstrcil, G. Lauder, R. Portugues, F. Engert, A novel mechanism for mechanosensory-based rheotaxis in larval zebrafish. *Nature* **547**, 445-448 (2017).
19. J. P. Durand, J. Parzefall, Comparative study of the rheotaxis in the cave salamander Proteus anguinus and his epigean relative Necturus maculosus (Proteidae, Urodela). *Behavioural Processes* **15**, 285-291 (1987).
20. D. R. Kobayashi *et al.*, "Going with the flow" or not: evidence of positive rheotaxis in oceanic juvenile loggerhead turtles (Caretta caretta) in the South Pacific Ocean Using Satellite Tags and Ocean Circulation Data. *PLoS One* **9**, e103701 (2014).
21. D. Rowat, M. Gore, Regional scale horizontal and local scale vertical movements of whale sharks in the Indian Ocean off Seychelles. *Fisheries Research* **84**, 32-40 (2007).
22. M. B. Orger, H. Baier, Channeling of red and green cone inputs to the zebrafish optomotor response. *Vis Neurosci* **22**, 275-281 (2005).
23. M. B. Orger, M. C. Smear, S. M. Anstis, H. Baier, Perception of Fourier and non-Fourier motion by larval zebrafish. *Nature Neuroscience* **3**, 1128-1133 (2000).
24. M. B. Orger, A. R. Kampff, K. E. Severi, J. H. Bollmann, F. Engert, Control of visually guided behavior by distinct populations of spinal projection neurons. *Nature Neuroscience* **11**, 327-333 (2008).
25. G. P. Arnold, RHEOTROPISM IN FISHES. *Biological Reviews* **49**, 515-576 (1974).
26. J. Bak-Coleman, D. Smith, S. Coombs, Going with, then against the flow: evidence against the optomotor hypothesis of fish rheotaxis. *Animal Behaviour* **107**, 7-17 (2015).
27. G. Valera *et al.*, A neuronal blueprint for directional mechanosensation in larval zebrafish. *Curr Biol* **31**, 1463-1475 e1466 (2021).

28. B. P. Chagnaud, C. Brucker, M. H. Hofmann, H. Bleckmann, Measuring flow velocity and flow direction by spatial and temporal analysis of flow fluctuations. *J Neurosci* **28**, 4479-4487 (2008).
29. M. Kulpa, J. Bak-Coleman, S. Coombs, The lateral line is necessary for blind cavefish rheotaxis in non-uniform flow. *J Exp Biol* **218**, 1603-1612 (2015).
30. J. Engelmann, W. Hanke, J. Mogdans, H. Bleckmann, Hydrodynamic stimuli and the fish lateral line. *Nature* **408**, 51-52 (2000).
31. S. Coombs, J. Bak-Coleman, J. Montgomery, Rheotaxis revisited: a multi-behavioral and multisensory perspective on how fish orient to flow. *J Exp Biol* **223**, (2020).
32. G. Vanwalleghem, K. Schuster, M. A. Taylor, I. A. Favre-Bulle, E. K. Scott, Brain-Wide Mapping of Water Flow Perception in Zebrafish. *J Neurosci* **40**, 4130-4144 (2020).
33. A. W. Visser, Hydromechanical signals in the plankton. *Marine Ecology Progress Series* **222**, 1-24 (2001).
34. W. M. Hamner, P. P. Hamner, S. W. Strand, R. W. Gilmer, Behavior of Antarctic Krill, Euphausia superba: Chemoreception, Feeding, Schooling, and Molting. *Science* **220**, 433-435 (1983).
35. S. Fossette *et al.*, Current-oriented swimming by jellyfish and its role in bloom maintenance. *Curr Biol* **25**, 342-347 (2015).
36. M. A. McManus, C. B. Woodson, Plankton distribution and ocean dispersal. *J Exp Biol* **215**, 1008-1016 (2012).
37. A. Genin, J. S. Jaffe, R. Reef, C. Richter, P. J. S. Franks, Swimming Against the Flow: A Mechanism of Zooplankton Aggregation. *Science* **308**, 860-862 (2005).
38. F. G. Michalec, I. Fouxon, S. Souissi, M. Holzner, Zooplankton can actively adjust their motility to turbulent flow. *Proc Natl Acad Sci U S A* **114**, E11199-E11207 (2017).
39. R. C. Fay, J. V. Johnson, Observations on the Distribution and Ecology of the Littoral Ascidians of the Mainland Coast of Southern California. *Bulletin, Southern California Academy of Sciences* **70**, 114-124 (1971).
40. A. Hernández-Zanuy, J. Carballo, Distribution and abundance of ascidian assemblages in Caribbean reef zones of the Golfo de Batabanó (Cuba). *Coral Reefs* **20**, 159-162 (2001).
41. C. C. Lambert, G. Lambert, Persistence and differential distribution of nonindigenous ascidians in harbors of the Southern California Bight. *Marine Ecology Progress Series* **259**, 145-161 (2003).
42. K. Ryan, I. A. Meinertzhagen, Neuronal identity: the neuron types of a simple chordate sibling, the tadpole larva of Ciona intestinalis. *Curr Opin Neurobiol* **56**, 47-60 (2019).
43. M. Nakagawa, T. Miyamoto, M. Ohkuma, M. Tsuda, Action Spectrum for the Photophobic Response of Ciona intestinalis (Ascidieacea, Urochordata) Larvae Implicates Retinal Protein. *Photochemistry and Photobiology* **70**, 359-362 (1999).
44. S. Kajiwara, M. Yoshida, Changes in Behavior and Ocellar Structure during the Larval Life of Solitary Ascidians. *Biol Bull* **169**, 565-577 (1985).
45. G. Zega, M. C. Thorndyke, E. R. Brown, Development of swimming behaviour in the larva of the ascidian Ciona intestinalis. *J Exp Biol* **209**, 3405-3412 (2006).
46. C. M. Young, F.-S. Chia, An experimental test of shadow response function in ascidian tadpoles. *Journal of Experimental Marine Biology and Ecology* **85**, 165-175 (1985).
47. A. Mathis *et al.*, DeepLabCut: markerless pose estimation of user-defined body parts with deep learning. *Nat Neurosci* **21**, 1281-1289 (2018).

48. A. Athira, D. Dondorp, J. Rudolf, O. Peytral, M. Chatzigeorgiou, Comprehensive analysis of locomotion dynamics in the protochordate Ciona intestinalis reveals how neuromodulators flexibly shape its behavioral repertoire. *PLoS Biol* **20**, e3001744 (2022).
49. T. Hiraiwa, Two types of exclusion interactions for self-propelled objects and collective motion induced by their combination. *Phys Rev E* **99**, 012614 (2019).
50. K. Ryan, Z. Lu, I. A. Meinertzhagen, The peripheral nervous system of the ascidian tadpole larva: Types of neurons and their synaptic networks. *J Comp Neurol*, (2017).
51. A. Konno *et al.*, Distribution and structural diversity of cilia in tadpole larvae of the ascidian Ciona intestinalis. *Dev Biol* **337**, 42-62 (2010).
52. H. Q. Terakubo *et al.*, Network structure of projections extending from peripheral neurons in the tunic of ascidian larva. *Dev Dyn* **239**, 2278-2287 (2010).
53. C. Anselmi, G. K. Fuller, A. Stolfi, A. K. Groves, L. Manni, Sensory cells in tunicates: insights into mechanoreceptor evolution. *Front Cell Dev Biol* **12**, 1359207 (2024).
54. J. Hoyer *et al.*, Polymodal sensory perception drives settlement and metamorphosis of Ciona larvae. *Curr Biol* **34**, 1168-1182 e1167 (2024).
55. G. Poncelet, L. Parolini, S. M. Shimeld, A microfluidic chip for immobilization and imaging of Ciona intestinalis larvae. *J Exp Zool B Mol Dev Evol*, (2024).
56. M. K. Wakai, M. J. Nakamura, S. Sawai, K. Hotta, K. Oka, Two-Round Ca(2+) transient in papillae by mechanical stimulation induces metamorphosis in the ascidian Ciona intestinalis type A. *Proc Biol Sci* **288**, 20203207 (2021).
57. A. Sakamoto *et al.*, The TRP channel PKD2 is involved in sensing the mechanical stimulus of adhesion for initiating metamorphosis in the chordate Ciona. *Dev Growth Differ* **64**, 395-408 (2022).
58. T. W. Chen *et al.*, Ultrasensitive fluorescent proteins for imaging neuronal activity. *Nature* **499**, 295-300 (2013).
59. K. Kolar, D. Dondorp, J. C. Zwiggelaar, J. Høyer, M. Chatzigeorgiou, Mesmerize is a dynamically adaptable user-friendly analysis platform for 2D and 3D calcium imaging data. *Nature Communications* **12**, (2021).
60. K. Ryan, Z. Lu, I. A. Meinertzhagen, The CNS connectome of a tadpole larva of Ciona intestinalis (L.) highlights sidedness in the brain of a chordate sibling. *Elife* **5**, (2016).
61. N. A. Khan *et al.*, Identification of drugs that restore primary cilium expression in cancer cells. *Oncotarget* **7**, 9975-9992 (2016).
62. E. J. Buskey, P. H. Lenz, D. K. Hartline, Sensory perception, neurobiology, and behavioral adaptations for predator avoidance in planktonic copepods. *Adaptive Behavior* **20**, 57-66 (2011).
63. S. Pigolotti, R. Benzi, Selective advantage of diffusing faster. *Phys Rev Lett* **112**, 188102 (2014).
64. D. Zhao *et al.*, Comparison of differentiation gene batteries for migratory mechanosensory neurons across bilaterians. *Evol Dev* **22**, 438-450 (2020).
65. A. Pasini *et al.*, Formation of the ascidian epidermal sensory neurons: insights into the origin of the chordate peripheral nervous system. *PLoS Biol* **4**, e225 (2006).
66. L. Desban *et al.*, Lateral line hair cells integrate mechanical and chemical cues to orient navigation. *bioRxiv*, 2022.2008.2031.505989 (2022).

67. J. Mogdans, H. Bleckmann, N. Menger, Sensitivity of Central Units in the Goldfish, Carassius auratus, to Transient Hydrodynamic Stimuli (Part 1 of 2). *Brain Behav Evolut* **50**, 261-272 (2008).
68. S. Künzel, H. Bleckmann, J. Mogdans, Responses of brainstem lateral line units to different stimulus source locations and vibration directions. *Journal of Comparative Physiology A* **197**, 773-787 (2011).
69. S. A. Torrence, R. A. Cloney, Nervous-System of Ascidian Larvae - Caudal Primary Sensory Neurons. *Zoomorphology* **99**, 103-115 (1982).
70. J. C. Marques, M. Li, D. Schaak, D. N. Robson, J. M. Li, Internal state dynamics shape brainwide activity and foraging behaviour. *Nature* **577**, 239-243 (2020).
71. A. Gordus, N. Pokala, S. Levy, S. W. Flavell, C. I. Bargmann, Feedback from network states generates variability in a probabilistic olfactory circuit. *Cell* **161**, 215-227 (2015).
72. S. W. Flavell *et al.*, Serotonin and the neuropeptide PDF initiate and extend opposing behavioral states in C. elegans. *Cell* **154**, 1023-1035 (2013).
73. E. Lottem *et al.*, Activation of serotonin neurons promotes active persistence in a probabilistic foraging task. *Nat Commun* **9**, 1000 (2018).
74. C. Kamiya *et al.*, Nonreproductive role of gonadotropin-releasing hormone in the control of ascidian metamorphosis. *Dev Dyn* **243**, 1524-1535 (2014).
75. N. Okawa *et al.*, Cellular identity and Ca(2+) signaling activity of the non-reproductive GnRH system in the Ciona intestinalis type A (Ciona robusta) larva. *Sci Rep* **10**, 18590 (2020).
76. T. Horie, M. Nakagawa, Y. Sasakura, T. G. Kusakabe, M. Tsuda, Simple motor system of the ascidian larva: neuronal complex comprising putative cholinergic and GABAergic/glycinergic neurons. *Zoolog Sci* **27**, 181-190 (2010).
77. T. Horie, T. Kusakabe, M. Tsuda, Glutamatergic networks in the Ciona intestinalis larva. *J Comp Neurol* **508**, 249-263 (2008).
78. K. Takamura, N. Minamida, S. Okabe, Neural map of the larval central nervous system in the ascidian Ciona intestinalis. *Zoolog Sci* **27**, 191-203 (2010).
79. E. R. Brown, A. Nishino, Q. Bone, I. A. Meinertzhagen, Y. Okamura, GABAergic synaptic transmission modulates swimming in the ascidian larva. *Eur J Neurosci* **22**, 2541-2548 (2005).
80. G. Zega *et al.*, Developmental expression of glutamic acid decarboxylase and of gamma-aminobutyric acid type B receptors in the ascidian Ciona intestinalis. *J Comp Neurol* **506**, 489-505 (2008).
81. J. Rudolf, D. Dondorp, L. Canon, S. Tieo, M. Chatzigeorgiou, Automated behavioural analysis reveals the basic behavioural repertoire of the urochordate Ciona intestinalis. *Sci Rep* **9**, 2416 (2019).
82. Z. Liang, D. C. Dondorp, M. Chatzigeorgiou, The ion channel Anoctamin 10/TMEM16K coordinates organ morphogenesis across scales in the urochordate notochord. *PLoS Biol* **22**, e3002762 (2024).
83. E. A. Pnevmatikakis, A. Giovannucci, NoRMCorre: An online algorithm for piecewise rigid motion correction of calcium imaging data. *J Neurosci Methods* **291**, 83-94 (2017).
84. E. A. Pnevmatikakis *et al.*, Simultaneous Denoising, Deconvolution, and Demixing of Calcium Imaging Data. *Neuron* **89**, 285-299 (2016).

85. A. Giovannucci *et al.*, CaImAn an open source tool for scalable calcium imaging data analysis. *Elife* **8**, (2019).
86. F. Pedregosa *et al.*, Scikit-learn: Machine Learning in Python. *J Mach Learn Res* **12**, 2825-2830 (2011).
87. B. Leggio *et al.*, MorphoNet: an interactive online morphological browser to explore complex multi-scale data. *Nat Commun* **10**, 2812 (2019).
88. F. Toschi, M. Sega, *Flowing Matter*. (2019).
89. S. van Teeffelen, H. Löwen, Dynamics of a Brownian circle swimmer. *Physical Review E* **78**, 020101 (2008).